

Use of nanostructured and modified TiO₂ as a gas sensing agent

R. Alves Junior^{1*}, H. P. A. Alves², J. M. Cartaxo³, A. M. Rodrigues³, G. A. Neves³, R. R. Menezes³

¹Federal University of Campina Grande, Materials Science and Engineering Postgraduate Program, 58429-900, Campina Grande, PB, Brazil

²Federal University of Rio Grande do Norte, Materials Science and Engineering Postgraduate Program, 59078-970, Natal, RN, Brazil

³Federal University of Campina Grande, Laboratory of Materials Technology, 58429-900, Campina Grande, PB, Brazil

Abstract

Titanium dioxide (TiO₂) has attracted interest for sensory applications due to its high surface area and the high density of active adsorption sites. This review shows the effect of the nanostructure, synthesis technique, operating temperature, target gas, and the impact of incorporating metallic elements on the detection properties of TiO₂. The studies showed that the TiO₂ gas detection process is closely related to surface reactions. Therefore, sensing properties, such as sensitivity, response time, and recovery, vary with factors that influence the surface reactions, such as chemical elements, morphology, microstructure of the depletion layer, and operating temperature.

Keywords: titanium dioxide, metallic elements, detection properties.

INTRODUCTION

The indispensable monitoring of the rapid expansion of ecological pollution, together with the need for more accurate information from technological advances, has made gas sensors increasingly essential [1-4]. Several applications, such as industrial manufacturing, aerospace, ocean exploration, environmental protection, medical diagnostics, and bioengineering, have been developing optimizations in sensors taking as main requirements high sensitivity, fast response, good selectivity, low-cost materials, and easy manufacturing [5-7]. Sensors can be made of various materials, depending on the purposes they serve, so it is essential to evaluate the physical and chemical properties of the compounds involved in the formation of gas sensors to achieve the best results in detecting multiple gases [8]. Generally, the types of gas sensors widely used can be classified into: metal oxide gas sensors, gas acoustic wave sensors, gas capacitance sensors, optical gas sensors, and calorimetric gas sensors [9]. Semiconductor metal oxide gas sensors are currently one of the most investigated gas sensor groups. They have attracted a lot of attention in gas detection in atmospheric conditions due to their low cost, flexibility in production, simplicity of use, and many application fields for detectable gases [9, 10].


Through conductive measurements, various metal oxides, such as Cr₂O₃, Mn₂O₃, Co₃O₄, NiO, CuO, SrO, In₂O₃, WO₃, TiO₂, V₂O₃, Fe₂O₃, GeO₂, Nb₂O₅, MoO₃, Ta₂O₅, La₂O₃, CeO₂, and Nd₂O₃ are used for the detection of combustible,

reducing, or oxidizing gases [11]. However, transition metal oxides perform better than pre-transition metal oxides (MgO, for example), as these oxides are relatively inert due to the large bandgap, while transition metal oxides behave differently because the energy difference between a cationic dⁿ configuration and a dⁿ⁺¹ or dⁿ⁻¹ configuration is often relatively small [12]. In this way, transition metal oxides are more sensitive than pre-transition metal oxides. The transition metal oxides with electronic configurations d⁰ (TiO₂, V₂O₅, WO₃) and d¹⁰ (ZnO, SnO₂) stand out for their gas sensor application, as they present less instability of their structures [13]. Titanium dioxide (TiO₂), in particular, has received attention since 1972, when Fujishima and Honda [14] discovered the photocatalytic division of water on a TiO₂ electrode under ultraviolet (UV) light. Studies have grown in the last decades for sensory applications since this semiconductor can present a high surface area (anatase phase), a high density of active adsorption sites, in addition to being non-toxic, biocompatible, free of photocorrosion, and economical [15-20]. Therefore, this work reviews the use of TiO₂ in gas sensing, highlighting its nanostructured use and application in composite systems.

TiO₂ STRUCTURE

TiO₂ can be found in three different phase structures, known as anatase, brookite, and rutile [21]. The anatase and rutile phases have a tetragonal crystalline structure (Figs. 1a and 1b), and brookite crystallizes in the orthorhombic system (Fig. 1c) [22], with an energy gap of 3.20 eV for anatase [23], 3.00 eV for rutile [24], and 3.14 eV for brookite [25]. Rutile is the stable phase; both anatase and brookite are metastable phases. However, at

*rubensalves.jr@hotmail.com

 <https://orcid.org/0000-0002-2259-1863>

room temperature, the process of converting anatase to rutile is so slow that it does not happen in practice [9]. Temperatures above 600 °C, depending on pressure, are necessary to promote this phase transformation that involves a solid-state diffusion of atoms in a process of nucleation and crystalline growth [19]. Anatase has lower surface energy than rutile, which favors its production at low temperatures [26]. Higher temperatures are required to obtain the rutile phase [27]. Understanding the process of transforming anatase into rutile and the variables that influence it is of great relevance since the type of crystalline phase is one of the main critical parameters determining the application of these materials [28]. Brookite is the least studied polymorph and has the least applicability. There is no agreement in the literature on the relative stability between brookite and anatase, and this is more likely to depend on the initial size of their particles [29]. Literature also relates the thermodynamically stable phase with the crystallite size: anatase is stable for crystallite sizes below 11 nm, brookite between 11 and 35 nm, and rutile for sizes greater than 35 nm [30].

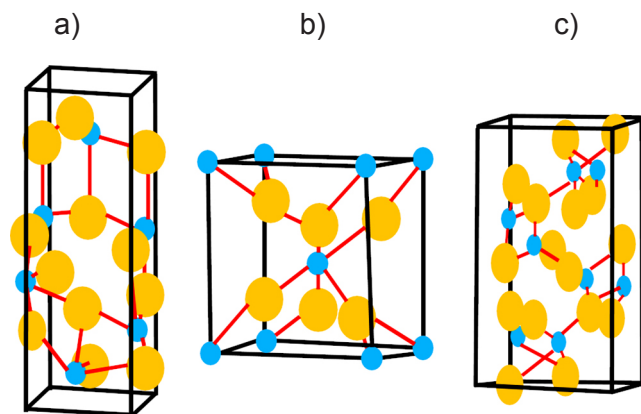


Figure 1: Structures of TiO_2 : a) anatase; b) rutile; and c) brookite. Orange spheres represent Ti atoms and the blue spheres represent O atoms.

In all three polymorphisms, each titanium atom (Ti^{4+}) coordinates with six oxygen atoms (O^{2-}) to form an octahedron [31]. The difference between the three crystalline structures is the deformation of each octahedron and its chains' organization. In the anatase phase, adjacent octahedra are shared by vertices. In the rutile phase, the edges are shared, and in the brookite phase, the vertices and edges are shared [28]. As confirmed by the stoichiometric theory for semiconductors, this type of crystal is rich in electrons and belongs to the n-type semiconductor [32]. Within this perspective, TiO_2 becomes a promising candidate for gas sensor applications. The TiO_2 gas sensor can detect different gases, including oxidizing gases and reducing gases, representing the increase and decrease in resistance, respectively [33]. Generally, the microscopic reactions between these gases and the TiO_2 surface can be very different according to the gas type, humidity, and environmental conditions. However, the following two

processes can summarize the detection mechanisms: the receptor process and the transducer process (Fig. 2) [34].

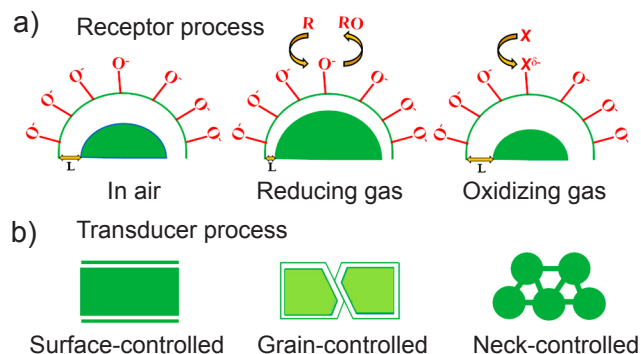


Figure 2: Schematic view of gas detection mode: a) receptor; and b) transducer.

The receptor process is related to the relationship between gas molecules and the TiO_2 surface [35]. The sensor permits the oxygen to be adsorbed on a superficial level (Fig. 2a) and then oxygen becomes charged negatively and the surface charge layer becomes depleted of electrons [9]. When a reducing gas is adsorbed on the oxygen (anionic) of the TiO_2 surface, electrons are injected on its surface, which reduces the depletion region and increases the conductivity of the surface. On the other hand, when oxidizing gases are adsorbed on the surface, they gain electrons from the adsorbed oxygen (anionic), which increases the depletion region and decreases conductivity [5]. It reaches a steady-state level, resulting in a decrease in the work function [36]. This function can also be modified by doping with a foreign receptor [37]. The transducer process involves electrons transmission of the semiconductor materials and converting electrons into external signals. This process is affected by electron transport modes, including surface-controlled, grain-controlled, and neck-controlled modes, as shown in Fig. 2b. The surface-controlled mode is generally related to compact layer structures [37]. Gases affect its geometric surface other than the bulk solution; thus, the compact layer's sensitivity is mainly determined by the thin film thickness [38]. On the contrary, all parts of the porous layer contact gases, which results in more activated sites in the porous layer. Because of this non-dense contact manner, each grain possesses a surface-depleted area [39]. The current has to pass through the intergranular contacts; therefore, the sensitivity of nanostructured TiO_2 is affected by the layer thickness and the pore size, and the carrier's diffusion length [5]. This resistance change induced by those interactions is considered one of the most critical gas sensors' characteristics [40]. The signal reflects the effects of the gas concentration and its diffusivity. Thus, at an equilibrium state in a gas sensor, the gas sensor's sensitivity is defined as the ratio of the resistance in the air to the resistance after exposure to the analytic gas [41].

NANOSTRUCTURED TiO₂

Significant progress has been made in recent years in the development of nanostructured materials for sensor applications [42-46]. In addition to the advantages inherent to the TiO₂, its nanostructures due to the large surface-to-volume ratio can significantly improve the sensors' sensitivity and selectivity compared to traditional materials, as their high surface area promotes an increase in the concentration of active sites for adsorption of oxygen [47]. Also, the availability of various nanostructures allows them to reach unique chemical, physical, and electronic properties [48, 49]. Furthermore, nanostructured TiO₂ can be prepared on a large scale in facile conditions and temperatures, facilitating low-cost manufacturing. Therefore, great interest has been shown in studies of TiO₂ with nanostructures, its transduction principle, and system simulation functions for sensor applications. Techniques commonly used to obtain TiO₂ nanostructures include sol-gel method [50], electrodeposition [51], chemical vapor deposition [52], physical vapor deposition [53], direct oxidation [54], hydrothermal [55], etc. These methodologies allow the production of TiO₂ in the crystalline structure of rutile or anatase, with varied morphology, from nanoparticles (1D) to three-dimensional(3D) nanostructures. Nanotubes (NTs) are one of the most widespread nanostructures for gas sensors. The primary way of obtaining them is by electrochemical oxidation reaction of a metallic titanium substrate [56-60]. More recently, Bindra and Hazra [61] used electrochemical anodization with a restricted supply of H₂O in the electrolyte to synthesize TiO₂ NTs, aiming to select organic vapors (methanol, ethanol, acetone, and 2-propanol). The formation of highly ordered and porous TiO₂ NTs was obtained, where diameters and lengths of the tubes were in the range of 110-150 nm and 2.5-2.7 μm, respectively. This type of structure offered a large surface area, which made it possible to adsorb organic vapors with a significant increase in the sensor's resistive response, even at low concentrations and low temperatures.

TiO₂ nanowires (NWs) are another typical one-dimensional structure with high sensitivity for detecting certain gaseous species [62, 63]. However, wet chemical synthesis methods, such as solid-liquid-vapor (SLV) [64-66], thermal oxidation [67, 68], hydrothermal [69], sol-gel [70, 71], pulsed laser deposition [72, 73], electrospinning [74], and anodizing method [75], have a high cost as they require more cleaning processes and the transfer of nanostructures on an appropriate substrate. Moreover, TiO₂ NWs are typically made in the form of a single nanowire. Despite its good detection characteristics, the practical application of available nanowire sensors has been limited by some severe disadvantages, including the difficulty of manufacture, low reliability, and high cost [76]. Lee *et al.* [63] were the pioneers in obtaining TiO₂ nanowires in monocrystalline mesh in the rutile

phase with an average diameter of 90 nm using the steam phase growth technique. In this work, the gas detection properties of sensors manufactured from networks of TiO₂ nanowires were comparable to that of alternative sensors that use other forms of TiO₂ and demonstrated that the networked TiO₂ nanowires represent a potential detection platform. In order to reduce the operational cost of synthesis by wet chemistry methods, Arachchige *et al.* [77] synthesized for the first time TiO₂ NWs by thermal oxidation directly on the alumina substrate, in which the thin layer of Ti was deposited on the substrate using little oxygen as a reducing gas (dry physical method). The NW of TiO₂ obtained had an average diameter of 20-40 nm and several micrometers in length. The gas detection measurements showed selectivity for ethanol and H₂ at an ideal temperature of 400 °C, and detection limits below 50 and 100 ppm for these gases, respectively.

A variation of the nanowire morphology for gas sensors is the nanorod (NR). They differ in length/diameter ratio and stiffness, as NRs have a smaller length/diameter ratio and greater stiffness than NWs. It is observed that TiO₂ NRs can be produced in the backbones of the Si NWs matrix through a process of pulsed chemical vapor deposition [78]. This work also provides evidence that uniform TiO₂ NRs can be grown on several surfaces. Wang *et al.* [79] reported the influence of temperature on the diameter of the TiO₂ NRs (rutile) when obtained by the physical vapor deposition. They showed the excellent response of this nanostructure to O₂ at room temperature, with a fast response time of 55 s and a recovery time of 51 s. TiO₂ NRs for acetone detection could also be obtained through electrospinning [80]. Bian *et al.* [80] studied TiO₂ NRs in a random network structure composed of a mixture of the anatase and rutile phases. The sensor showed high sensitivity ($R_{air}/R_{gas} \approx 20$), good selectivity, and reproducibility for acetone with the response and recovery time of 11 and 8 s, respectively, at 500 °C. Electrospinning was also used for the synthesis of TiO₂ nanofibers. Park *et al.* [81] reported that a random network structure of several layers of titanium dioxide nanofibers can be manufactured by calcination (400, 600, and 800 °C) of the electrospun hybrid fibers of TiO₂/PVP. After calcination at 600 °C, this structure displayed the highest gas response ($R_{air}/R_{gas} \approx 4.3$) in a concentration of 25 ppm CO at 200 °C, compared to those calcined at 400 °C ($R_{air}/R_{gas} \approx 3.1$) and 800 °C ($R_{air}/R_{gas} \approx 2.2$). The sensor based on TiO₂ nanofibers calcined at 600 °C showed a gas response to CO concentration as low as 1 ppm. This ability of TiO₂ nanofibers to detect low concentrations of CO was attributed to the unique geometry and distribution characteristics of the TiO₂ nanofiber.

In addition to the one-dimensional nanostructures, there is a great deal of attention from researchers regarding TiO₂ nanoparticles. The TiO₂ microsphere's geometry can be controlled by adding different chemicals in the titanium precursors' aqueous solutions. Navale *et al.* [82] obtained TiO₂ nanoparticles (NPs) using a titanium glycolate precursor using a simple hydrothermal route, which their chemosensitive activity was considered for various target

gases. The gas detection results demonstrated that the TiO₂ NP-based sensor has high selectivity for CH₃COCH₃ and is capable of detecting its concentration up to the limit of ppb level at an operating temperature of 270 °C. Taha et al. [49] prepared thick films of titanium dioxide nanoparticles, titanium dioxide nanowires, and titanium dioxide nanotubes to analyze three different TiO₂ nanostructures about the detection parameters, such as operating temperature, response/recovery time, and absorption capacity of alcohol vapors, such as methanol, ethanol, and propanol vapors at a low concentration level (10 ppm). The results showed that the nanostructured morphologies exhibit different behaviors concerning sensitivity, operating temperature, and response/recovery time. NPs showed the lowest operating temperature for alcohols than the rest of the nanostructure. NWs have an excellent response to alcohols, but the recovery was better observed in NPs' nanostructure. Table I lists different types of TiO₂ nanostructures and their responses to different types of gases.

TiO₂-DOPING OR ASSISTANT METALS

The introduction of some defects in the nanometer scale, such as noble metals, can increase the responses of TiO₂ sensors to detect gases. According to the metal,

atoms modify the surface sensitization and doping [95]. Noble metals (e.g., Au, Pd, Pt) are often used to improve surface sensitivity and selectivity because their Fermi level is usually lower than TiO₂ [96]. The detection property rises with an increase in adsorption sites for incoming gas molecules. The selectivity increases due to these metals' catalytic effect since much of the catalytic reactions' efficiency occur on the material's surface. The transition metals (Co and Zr, for example) are more used as doping elements, as they change the structure of TiO₂ since they have similarities with the atomic radius of Ti. However, it generates distortions in the crystalline network and functional defects such as oxygen vacancy (V_o) or interstitial titanium (Ti^{δ+}), which significantly increases the number of oxygen adsorption sites around transition metal atoms [97].

Bastakoti et al. [98] found that the introduction of platinum (Pt) on the surface of the mesoporous TiO₂ increased the sensor's sensitivity to acetaldehyde at room temperature, as well as, the sensor exhibited a higher adsorption rate and excellent absorption of acetaldehyde adsorption compared to pure mesoporous TiO₂. The use of Pt in TiO₂ is also reported as a noble metal that favors the sensitivity of TiO₂ for the detection of other gases [99, 100]. Xing et al. [101] synthesized via hydrothermal method

Table I - Types of TiO₂ nanostructures and their responses to different types of gases.

Synthesis technique	Sensitive gas	Operating temperature	Detection limit range	Nanostructure	Response time	Ref.
Spin-coating	NH ₃ , H ₂ S, NO, CH ₃ OH, C ₂ H ₅ OH	200 °C	20-100 ppm	Nanoparticle (crystal)	-	[83]
Sol-gel	Petroleum gas	-	-	Nanoparticle (crystal)	240 s	[84]
Magnetron reactive sputtering	NH ₃	30 °C	5-100 ppm	Nanoparticle (crystal)	34 s	[85]
Thermal oxidation	Ethanol, H ₂	400 °C	50-100 ppm	Nanowire	120-240 s	[77]
Ti deposition	CO	400 °C	1 ppm	Nanowire	-	[63]
Hydrothermal	Organic gases	500 °C	-	Nanotube	-	[86]
Hydrothermal	NO ₂	180 °C	100 ppm	Nanowire	10 s	[87]
Hydrothermal	Toluene	500 °C	100 ppm	Nanotube	-	[88]
Hydrothermal	H ₂	200 °C	500 ppm	Nanorod	-	[89]
Hydrothermal	Triethylamine	290 °C	100 ppm	Nanorod	2 s	[90]
Anodizing	Formaldehyde	30 °C	10-50 ppm	Nanotube	-	[91]
Anodizing	NH ₃	30 °C	150 ppm	Nanotube	-	[92]
Electron beam lithography	Ethanol	300 °C	0.2 µg	Nanowire	3.2 s	[93]
Acid vapor oxidation	O ₂	30 °C	16%	Nanorod	55 s	[79]
Electrospinning	Acetone	500 °C	150 ppm	Nanorod	11 s	[80]
Electrospinning	CO	200 °C	25 ppm	Nanofiber	3.8 s	[81]
Electrospinning	Ethanol	300 °C	100 ppm	Nanofiber	15 s	[94]

sensors of mesoporous TiO₂ and Pt-doped mesoporous TiO₂. The sensors' gas detection performance showed favorable selectivity, good gas response value, fast response/recovery time, low detection concentration, and good long-term stability for acetone (300 °C). TiO₂ doped with 0.5% Pt showed the highest gas response value of 29.51 for 200 ppm acetone at 300 °C, that is, 5.2 times greater than that of a gas sensor based on pure TiO₂ (5.67). The authors [101] attributed this better performance of the Pt/TiO₂ sensor to the catalytic effect of Pt, which increases the ability to absorb oxygen molecules and accelerate the reaction between adsorbed oxygen species (O_x⁻) and acetone gas molecules, as well as the fact that Pt atoms introduce an intermediate energy level in the bandgap, making it easier for excited electrons to migrate from the valence band to conduction band. Abe *et al.* [102] also reported that the introduction of Pt on the surface of TiO₂ favors the detection of gases (hydrogen, carbon monoxide). They synthesized films of TiO₂ nanotubes (NTs) with Pt and by anodic oxidation and atomic layer deposition. When exposed to H₂ gas and 1% CO diluted in nitrogen at 300 °C, the Pt nanoparticles promoted the dissociative adsorption of H₂ gas molecules on the surface of the TiO₂ NTs, leading to an increase of 7 order of magnitude in the sensor response. Rane *et al.* [103] revealed that Pt in TiO₂ films, through photochemical reduction, is responsible for decreasing the operating temperature of the gas sensor (≥90 °C) for different test gases, such as hydrogen, ammonia, and ethanol.

By changing the function of TiO₂ by noble metals, they can be categorized into 'chemical sensitization' and 'electronic sensitization', in which chemical sensitization manifests itself mainly as an overflow effect without changing the resistance of TiO₂. In contrast, electronic sensitization can be attributed to the overflow of the target gas in the noble metals on the TiO₂ surface and the decrease in the resistance of TiO₂ by electron transfer at the interface [95, 104]. Incorporating Au into the TiO₂ surface is an example of chemical sensitization, as Au favors the connection between the molecules of the target gases and the metallic network. Abbasi and Sardroodi [105] made Au/TiO₂ sensors for the detection of NO₂, where they revealed that the atoms that make up the target gas chemically bond to Au. This agrees well with Chomkitichai *et al.* [106], who concluded that the H₂ gas detection performance increased with the introduction of 0 to 0.75% Au in TiO₂. The use of nanostructured noble metals as TiO₂'s assistant metals optimizes the sensor responses [107]. Mintcheva *et al.* [107] synthesized nanomaterials prepared via irradiation of TiO₂ nanopowders by pulsed laser in milliseconds followed by the deposition of Au nanoparticles and observed that the synthesis method led to the formation of Ti³⁺ ions and oxygen vacancies on the surface, which appear to be related to nucleation and growth of Au nanoparticles deposited on the Ti support. Thus, laser-irradiated semiconductor nanomaterials improved the sensor's sensitization and adjusted the selectivity. Nikfarjam *et al.* [74] analyzed the detection of TiO₂-aligned nanofibers doped with Au nanoparticles obtained by electrospinning

equipped with electrostatic fields for CO detection. Sensor response and recovery times have been improved with the introduction of Au nanoparticles. The addition of Au in pure TiO₂ (300 °C) nanoparticles, when exposed to a concentration of 200 ppb of CO, increased the response from 190% to 597% and decreased the recovery time. The authors [74] revealed that Au nanoparticles act as catalysts, form a Schottky barrier between them and TiO₂, and reduce the activation energy required for the interaction between CO and O, which improves the sensor's response. The same gas detection mechanism was exposed by Zhang *et al.* [108], who synthesized TiO₂ hierarchical architectures and Au-loaded TiO₂ for the detection of toluene. The results indicated that Au improved the performance of the TiO₂ sensor, especially the 5% Au/TiO₂ sensor that showed a better response (7.3), short response (4 s) and recovery (5 s) times, excellent repeatability, and stability at 100 ppm toluene at 375 °C.

Nataraj *et al.* [109] analyzed the CO detection properties of Ag/TiO₂ sensors using an orthogonal matrix of experiments, in which the annealing temperature (200, 250, and 300 °C), the amount of dopant (0.025, 0.050, and 0.075 atomic ratios), and the concentration of CO gas (1, 3, and 5 ppm). Silver loaded in TiO₂ provides a more active site for sorption of gas, as well as Ag also acts as a catalyst to increase the adsorption of gas molecules and accelerate the exchange of electrons between the sensor and the test gas. Wang *et al.* [110] also showed that an Ag (2 mol%) Ti modified NP has excellent sensory properties, such as sensitivity (SR ~13.9), response and recovery times (11 s), and good long-term stability (30 days) for 100 ppm acetone. The improvement of detection properties was attributed to the electronic sensitization mechanism since the resistance of TiO₂ (R_{air} ~465 MΩ) is more significant than Ag/TiO₂ (R_{air} ~133 MΩ). TiO₂ gas sensors doped with noble materials usually only show excellent results at elevated temperatures. However, Rahbarpour *et al.* [111] analyzed the sensitivity versus operating temperature studies in an Ag/TiO₂ to detect methanol vapor. The operating temperature of this type of sensor depends on the gas concentration, such that the higher the target gas concentration, the lower the operating temperature. The results were described based on the calculation of the oxygen coverage of the silver surface under different conditions. Şennik *et al.* [112] studied the improvement of the TiO₂ NRs gas detection parameters through the Pd addition process. When Pd nanoparticles were added to the TiO₂ NR sensor, there is a ~250 response when exposed to 1000 ppm of hydrogen at 30 °C; pure TiO₂ had no response at these conditions. When both were tested in this concentration of target gas at 200 °C, the TiO₂ Pd/NRs showed a sensitivity 35 times better than the TiO₂ NRs sensor. This improvement in temperature decrease for hydrogen detection was justified as the particles of Pd dispersed on the surface form active sites that increase hydrogen absorption since the Pd behaves as a 'collector of hydrogen', reducing the working temperature to 30 °C. Pan *et al.* [113] showed that the TiO₂ nanofilm sensors

with Pd (1 wt%) responded quickly to the change in CO concentration since CO molecules were more easily absorbed and, consequently, activated in the surface of the PdO, and then transferred to the grain surface of the TiO₂ film to react with the chemically adsorbed oxygen species. The depletion layer became stronger due to the unoccupied d orbital and the unrelated valence electron of the palladium ion (Pd²⁺), which made the PdO a strong electron acceptor, removing electrons from TiO₂. In this same perspective, Zhang et al. [114] synthesized Pd-TiO₂/MoS₂ ternary nanocomposite films to detect benzene gas at room temperature. They confirmed that Pd has a significant electronic sensitization effect and availability of active sites for benzene gas adsorption. However, they clarified that contents above 4 wt% of Pd cause a decrease in the sensor's sensitivity.

When transition metals are used to dope TiO₂, other mechanisms are predominant. When TiO₂ is doped with Co³⁺, for instance, Co replaces part of the Ti network; therefore, it changes the network parameter and transforms positive and negative charge centers of the octahedron [97], which significantly increases the number of oxygen adsorption sites around Co atoms. In this perspective, Fomekong and Saruhan [115] reported that replacing Ti⁴⁺ with Co³⁺ creates oxygen vacancies and promotes the transformation of anatase to rutile. Likewise, they said that TiO₂ doped with Co reveals a conductive p-type behavior that produces an enhanced NO₂ response at 600 °C under air as a carrier gas. Kumar et al. [116] synthesized TiO₂ films doped with different Mg concentrations (1, 3, 5, and 7 wt/v% of Mg) using the sol-gel spin coating technique. When deposited on silicon substrates, these films were tested for CO detection (120 to 920 ppm). It was observed that the electron density of the crystalline network increased due to the incorporation of Mg²⁺ ions, causing a decrease in the resistivity of TiO₂ doped with Mg when compared to pure TiO₂. As for the detection of CO, the composite film with the highest level of Mg doping (7 wt/v%) obtained the best responses since it presented the lowest sensitivity (0.304 MΩ/ppm) and the shortest response and recovery time (41 and 22 s, respectively).

Chromium (Cr) for having an atomic radius similar to Ti (Cr³⁺=0.61 Å, Ti⁴⁺=0.60 Å) is a non-noble metal suitable for application as a TiO₂ dopant for gas detection since Cr³⁺ can replace Ti⁴⁺ in the TiO₂ network to form additional defects (such as oxygen vacancies and interstitial Ti atoms), which can alter the electronic structure of TiO₂ and transform TiO₂ into the p-type semiconductor. Based on its p-type conductivity, Cr³⁺ doped TiO₂ exhibits better sensitivity to H₂ [117]. Xie et al. [118] also synthesized Cr/TiO₂ films. Different Cr concentrations (1, 3, 5, 10 at%) were used and detection of H₂ was performed at different temperatures (300 to 500 °C). With the addition of chromium dopant, the interpretation of p-type behavior was associated with the presence of acceptor states. Generally, chromium dopant affects the electronic structure of TiO₂ and forms acceptor levels located in the bandgap. In this work, the

TiO₂ gas sensor doped with 5 at% of Cr showed the best gas detection performance at 500 °C. The response value is 152.65, the response/recovery time is fast (142/123 s) when exposed to 1000 ppm of hydrogen and it has good selectivity to hydrogen. The effectiveness in improving gas detection caused by the introduction of Cr in the TiO₂ structure can also be seen for other gases, as reported by Sertel et al. [119], which observed that the response of the sensor to propane gas in concentrations of 250, 500, and 1000 ppm at an operating temperature of 300 °C increases with increasing Cr content. The use of Cr as a TiO₂ doping element for CO₂ detection was reported by Mardare et al. [120], which observed an increase of 9 times in the response for CO₂ detection (10000 ppm) when TiO₂ was doped with 4 at% Cr at 55 °C. However, this same research group observed that TiO₂ doped with Fe has excellent sensitivity to high concentrations of CO₂ at room temperature, although the detection mechanism employed is different due to the diverse nature of the crystalline structure [121]. It is noted that TiO₂ films doped with Cr have an organized crystalline structure, in which electrical transport takes place through the grain, while TiO₂ films doped with Fe are amorphous. At low concentrations of Fe, it was observed that the change in conductivity in the presence of CO₂ occurred through the n-type conductivity. However, with the increase in Fe's concentration, the increase in conductivity is attributed to the decrease in the charge carriers, which leads to a rise in the level of Fermi in the presence of CO₂. Tong et al. [122] have also studied the use of Fe as a doping element of TiO₂. They analyzed the film performance of Fe-doped TiO₂ nanotubes to detect H₂S at low working temperatures. The results showed that Fe does not alter the surface morphology of the film since Fe ions are part of the TiO₂ structure, favoring the reduction of the Fermi level, which consequently reduces the thermal excitation energy used to increase the free-electron electricity in the TiO₂ conduction band, which implied in reducing the sensor's working temperature. Also, Fe/TiO₂ nanotube films showed a sensor response 3.03 times greater than TiO₂ nanotubes for 50 ppm H₂S at 100 °C. In [123], two mechanisms have been reported to explain the improvement in the detection properties of Fe-TiO₂/MoS₂ films to ethanol at room temperature when compared to pure TiO₂. Firstly, the doping of Fe³⁺ in TiO₂ can produce more oxygen vacancy due to Fe³⁺ replacing Ti⁴⁺, which is useful for improving ethanol detection performance, as an impurity energy level is created by doping with Fe³⁺, which reduces the TiO₂ bandgap. Another possible mechanism for the Fe-TiO₂/MoS₂ sensor is the p-n heterojunctions generated at the n-type Fe-TiO₂ and p-type MoS₂ interface, which can promote the reaction between the adsorbed oxygen and the detection film. As the Fermi level of MoS₂ is greater than that of Fe-TiO₂, electrons flow from MoS₂ to Fe-TiO₂ and holes flow from Fe-TiO₂ to MoS₂ until the Fermi level reaches the equilibrium. Therefore, a depletion layer forms at the interface of Fe-TiO₂ and MoS₂, where electrons accumulate on the side of Fe-TiO₂ and holes

accumulate on MoS_2 . In this way, the sensor's resistance decreases in the air and increases in the ethanol gas due to the modulation of the depletion layer's width [123].

The doping of TiO_2 with 0.5 mol% Ni presented another H_2 gas detection mechanism [124]. The authors suggested that the best performance in the sensor's response (72%) of Ni (0.5 mol%)/ TiO_2 in detecting 10000 ppm of H_2 at 600 °C was based on the higher formation of n-junction numbers present between the anatase and rutile phases. This behavior was observed only at this concentration of Ni. This behavior can be explained by forming a Schottky barrier at the anatase/rutile junction. They clarify that electrons flow from the anatase to the rutile when an electric field is applied to this composition. The holes flow in the opposite direction, which brings a balance at the Fermi level, and generates electron depletion in the anatase/rutile interface layer. This interaction facilitates more significant oxygen adsorption on the sensor surface due to more active reaction sites. Therefore, when in contact with H_2 , more electrons are released back into the conduction band, eventually leading to an increased sensor response. Vijayalakshmi and Monamary [125], on the other hand, attributed the improvement in the performance of the Ni/ TiO_2 sensor for the detection of 400 sccm of H_2 at room temperature to the behavior of the p-type semiconductor. The acceptor impurity level in p-type Ni/ TiO_2 films generates trapped hole centers since the presence of Ni as an impurity in the TiO_2 network is also known to create insufficient oxygen since it induces an impurity level when Ni/ TiO_2 film adsorbs a certain amount of hydrogen and the bandgap increases, which increases the sensor resistance. Another doping metal is niobium (Nb). Galstyan *et al.* [126] indicated that the detection performance of TiO_2 nanotubes, in terms of response magnitude, ideal operating temperature, and baseline conductivity, can be optimized with the doping of Nb for the detection of some gases, such as H_2 , CO, acetone, and ethanol. Galstyan *et al.* [127] reported the analysis of Nb-doped TiO_2 nanotubes obtained through anodic oxidation to detect dimethylamine (DMA), which is an essential indicator for checking the degradation of seafood. Detection measurements of TiO_2 nanotubes and TiO_2/Nb nanotubes were performed at 300 °C for 5, 10, 25, and 50 ppm DMA. However, the TiO_2 nanotubes showed only sensitivity from 10 ppm. TiO_2/Nb nanotubes showed a better response than TiO_2 NTs, related to sensor response, response time, and recovery time, since the Nb^{5+} ions, which are present in the cationic sites replacing Ti, act as donor center and promote the gas adsorption process on the material, improving the structure response. However, when Nb was introduced to TiO_2 in a structure similar to a Pt/Nb- TiO_2 /Pt capacitor to detect hydrogen gas, an unexpected result occurred. The response of the sensor with Nb-doped TiO_2 film was lower compared to the non-doped Pt/ TiO_2 /Pt sensor, which exhibited the highest response and the shortest response time for 1000 ppm of hydrogen at 100 °C [128]. This behavior was attributed to

a decrease in surface roughness and the porosity of TiO_2 films doped with Nb that limited the gas diffusion rate.

Abbasi and Sardroodi [129] investigated the adsorption behavior of the O_3 molecule in N and Zr/N doped TiO_2 anatase nanoparticles. Although the O_3 molecule is poorly adsorbed in the pure nanoparticle (no doped), it tends to have chemical adsorption in the nanoparticles doped with N. The results suggested that the titanium sites five times coordinated are the preferential site of adsorption of the molecules of O_3 , when compared with the sites of nitrogen and oxygen. The adsorption of the ozone molecule on the N-doped particle was energetically more favorable than the adsorption on the non-doped particle, indicating the dominant effects of nitrogen doping on the performance of the nanoparticles. Pan *et al.* [130] observed that nanocomposites of TiO_2 nanospheres/tungsten diselenide (WSe_2) nanofibers produced by a hydrothermal route presented excellent sensory sensing responses (43.8 to 100 ppm) and response/recovery time (2/1 s at 30 ppm) at room temperature. The predominant factor for the improvement in the sensory properties of TiO_2 with the introduction of WSe_2 is the fact that WSe_2 acts as a transmission path for charge transfer owing to its high carrier mobility and small natural bandgap as well as the van der Waals interaction between TiO_2 and WSe_2 , which facilitates the hybridization of the two materials, due to the large specific surface area of WSe_2 nanosheets and the uniform adhesion of the TiO_2 nanospheres. This nanocomposite provides many active sites for the adsorption of ethanol gas, which is a crucial element to increase the ethanol detection property of the $\text{TiO}_2/\text{WSe}_2$ compound. This contact between the components provides the formation of heterojunction at the interface of p-type WSe_2 and n-type TiO_2 . This interface does not only function as a catalytic center where ethanol molecules are readily adsorbed on it, but it also promotes the electron transfer rate and rapid oxidation of ethanol gas. The TiO_2 in this same structure (nanospheres) was used to manufacture TiO_2 /tin disulfide (SnS_2) nanocomposites [131]. The authors showed that the use of TiO_2 nanospheres in SnS_2 increases the moisture detection properties in high response, low hysteresis, rapid response and recovery times, and good reproducibility. This nanocomposite has more active sites and nanopores than the isolated elements, which can provide high surface exposure for water molecules' adsorption. Although SnS_2 has greater moisture detection capacity than TiO_2 due to the different hydrophilic functional groups, the nanomaterial's synergetic effect gives the $\text{SnS}_2/\text{TiO}_2$ sensor better detection properties, reaching an impedance response of up to 2000 and a sensitivity of 442000 $\Omega/\%RH$. Finally, Table II summarizes recent research on several metals used as dopants for TiO_2 with the possible application of gas sensors.

CONCLUSIONS

The reports indicated that the variation in the synthesis

Table II - TiO₂ doped with various metals for application in gas sensors.

Material	Synthesis method	Temperature	Gas concentration	Sensitive gas	Sensor response	Ref.
Fe/TiO ₂	Mechanochemical grinding	270 °C	500 ppm	H ₂	94.1% ^a	[132]
Co/TiO ₂	Evaporation-induced self-assembly	30 °C	1000 ppm	H ₂	1.1x10 ^{3b}	[133]
Nb/TiO ₂	Hydrothermal	30 °C	8000 ppm	H ₂	98.9% ^c	[134]
Cr/TiO ₂ NT	Anodizing	400 °C	100 ppm	CO	3.4 ^b	[135]
Ni/TiO ₂	Electrospray	302 °C	100 ppm	Xylene	4.4 ^b	[136]
W/TiO ₂	Sol-gel+spin coating	200 °C	10000 ppm	CO ₂	1.34 ^b	[137]
W/TiO ₂	Hydrothermal	240 °C	500 ppm	Acetone	173.67 ^b	[138]
Cr/TiO ₂	Confocal sputtering	300 °C	1000 ppm	Propane	67.55% ^c	[119]
Zn/TiO ₂	Spin coating	30 °C	1.5 vol%	LPG	0.462 ^b	[139]
Sn/TiO ₂	Spray pyrolysis	300 °C	100 ppm	H ₂	77 ^b	[140]
Y/TiO ₂	Spin coating	250 °C	300 ppm	NH ₃	125 ^d	[141]
Mn/TiO ₂	Hydrothermal	30 °C	20 ppm	NH ₃	127.39 ^b	[142]
N/TiO ₂	Evaporation	30 °C	250 ppm	Acetone	17.6 ^b	[143]

$$^a = (1 - R_{\text{gas}}/R_{\text{air}}) \cdot 100; ^b = R_{\text{air}}/R_{\text{gas}}; ^c = [(R_{\text{air}} - R_{\text{gas}})/R_{\text{gas}}] \cdot 100; ^d = [(R_{\text{air}} - R_{\text{gas}})/R_{\text{gas}}]$$

technique, morphology, operating temperature, and introduction of metallic elements modify the detection mechanism of TiO₂ when exposed to the most varied target gases. It is noteworthy that the large surface/volume ratio found in the nanostructures and the use of auxiliary metals positively alters the detection properties in such a way as to increase the sensitivity and reduce the response and recovery times when compared with pure TiO₂. These changes can be due to changes in the reaction surface of TiO₂ and the creation of adsorption sites in the crystalline structure of titanium dioxide.

ACKNOWLEDGEMENTS

Authors acknowledge Brazilian agencies Coordenação de Aperfeiçoamento de Pessoal e Nível Superior - Brasil (CAPES) - Finance Code 001 (scholarship granted to Rubens Alves Junior) and CNPq (grants Nos. 308822/2018-8 and 420004/2018-1) for support the research.

REFERENCES

- [1] H. Akimoto, *Science* **302** (2003) 1716.
- [2] I.F. Akyildiz, W. Su, Y. Sankarasubramaniam, E. Cayirci, *Comput. Netw.* **38** (2002) 393.
- [3] D. Kwak, Y. Lei, R. Maric, *Talanta* **204** (2019) 713.
- [4] S. Pandey, K.K. Nanda, *ACS Sens.* **1** (2016) 55.
- [5] J. Bai, B. Zhou, *Chem. Rev.* **114** (2014) 10131.
- [6] S.S. Shendage, V.L. Patil, S.A. Vanalakar, S.P. Patil, N.S. Harale, J.L. Bhosale, J.H. Kim, P.S. Patil, *Sens. Actuator B Chem.* **240** (2017) 426.
- [7] F. Yang, J. Zhu, X. Zou, X. Pang, R. Yang, S. Chen, Y. Fang, T. Shao, X. Luo, L. Zhang, *Ceram. Int.* **44** (2018) 1078.
- [8] I. Kim, W.-Y. Choi, *Int. J. Nanotechnol.* **14** (2017) 155.
- [9] J.M. Rzaizj, A.M. Abass, *J. Chem. Rev.* **2** (2020) 114.
- [10] G. Korotcenkov, *Mater. Sci. Eng. B* **139** (2007) 1.
- [11] E. Kanazawa, G. Sakai, K. Shimano, Y. Kanmura, Y. Teraoka, N. Miura, N. Yamazoe, *Sens. Actuator B Chem.* **77** (2001) 72.
- [12] V.E. Henrich, P.A. Cox, *The surface science of metal oxides*, Cambridge Un. Press, New York (1996).
- [13] C. Wang, L. Yin, L. Zhang, D. Xiang, R. Gao, *Sensors* **10** (2010) 2088.
- [14] A. Fujishima, K. Honda, *Nature* **238** (1972) 37.
- [15] M.R. Al-Mamun, S. Kader, M.S. Islam, M.Z.H. Khan, *J. Environ. Chem. Eng.* **7** (2019) 103248.
- [16] A.M. Amanulla, R. Sundaram, *Mater. Today Proc.* **8** (2019) 323.
- [17] S.-J. Bao, C.M. Li, J.-F. Zang, X.-Q. Cui, Y. Qiao, J. Guo, *Adv. Funct. Mater.* **18** (2008) 591.
- [18] L. Gao, C. Yin, Y. Luo, G. Duan, *Nanomaterials* **9** (2019) 493.
- [19] D.A.H. Hanaor, C.C. Sorrell, *J. Mater. Sci.* **46** (2011) 855.
- [20] F. Li, H. Song, W. Yu, Q. Ma, X. Dong, J. Wang, G. Liu, *Mater. Lett.* **262** (2020) 127070.
- [21] A. Yamakata, J.J.M. Vequizo, *J. Photochem. Photobiol. C Photochem. Rev.* **40** (2019) 234.
- [22] T.R. Esch, I. Gadaczek, T. Bredow, *Appl. Surf. Sci.* **288** (2014) 275.
- [23] E. Zhang, Y. Pan, T. Lu, Y. Zhu, W. Dai, *Appl. Phys. A* **126** (2020) 606.
- [24] D. Zhang, S. Dong, *Prog. Nat. Sci. Mater. Int.* **29** (2019)

- 277.
- [25] C.G. Ezema, A.C. Nwanya, B.E. Ezema, M. Maaza, P.O. Ukoha, F.I. Ezema, J. Solid State Electrochem. **21** (2017) 2655.
- [26] M. Cargnello, T.R. Gordon, C.B. Murray, Chem. Rev. **114** (2014) 9319.
- [27] Y. Wang, L. Zhang, K. Deng, X. Chen, Z. Zou, J. Phys. Chem. C **111** (2007) 2709.
- [28] O. Carp, C.L. Huisman, A. Reller, Prog. Solid State Chem. **32** (2004) 33.
- [29] H. Zhang, J.F. Banfield, J. Phys. Chem. B **104** (2000) 3481.
- [30] S.-D. Mo, W.Y. Ching, Phys. Rev. B **51** (1995) 13023.
- [31] M. Pelaez, N.T. Nolan, S.C. Pillai, M.K. Seery, P. Falaras, A.G. Kontos, P.S.M. Dunlop, J.W.J. Hamilton, J.A. Byrne, K. O'Shea, M.H. Entezari, D.D. Dionysiou, Appl. Catal. B Environ. **125** (2012) 331.
- [32] A. Sclafani, J.M. Herrmann, J. Phys. Chem. **100** (1996) 13655.
- [33] P. Shankar, J.B.B. Rayappan, Sci. Lett. J. **4** (2015) 126.
- [34] A. Oprea, U. Weimar, Anal. Bioanal. Chem. **411** (2019) 1761.
- [35] T.L. Thompson, J.T. Yates, Chem. Rev. **106** (2006) 4428.
- [36] S. Ma, M.E. Reish, Z. Zhang, I. Harrison, J.T. Yates, J. Phys. Chem. C **121** (2017) 1263.
- [37] D.E. Williams, Sens. Actuator B Chem. **57** (1999) 1.
- [38] E. Comini, Anal. Chim. Acta **568** (2006) 28.
- [39] S. Capone, A. Forleo, L. Francioso, R. Rella, P. Siciliano, J. Spadavecchia, D.S. Presicce, A.M. Taurino, J. Optoelectron. Adv. Mater. **5** (2003) 1335.
- [40] N. Yamazoe, G. Sakai, K. Shimanoe, Catal. Surv. Asia **7** (2003) 63.
- [41] S. Ahlers, G. Müller, T. Doll, Sens. Actuator B Chem. **107** (2005) 587.
- [42] G. Atanasova, A.O. Dikovska, T. Dilova, B. Georgieva, G.V. Avdeev, P. Stefanov, N.N. Nedyalkov, Appl. Surf. Sci. **470** (2019) 861.
- [43] N. Barsan, D. Koziej, U. Weimar, Sens. Actuator B Chem. **121** (2007) 18.
- [44] E. Comini, D. Zappa, Woodhead Publ. Ser. Electron. Opt. Mater., Woodhead Pub. (2020) 161.
- [45] W. Guan, N. Tang, K. He, X. Hu, M. Li, K. Li, Front. Chem. **8** (2020) 76.
- [46] D. Nunes, A. Pimentel, A. Gonçalves, S. Pereira, R. Branquinho, P. Barquinha, E. Fortunato, R. Martins, Semicond. Sci. Technol. **34** (2019) 43001.
- [47] H.S. Ferreira, M.C. Rangel, Quím. Nova **32** (2009) 1860.
- [48] S.H. Salman, A.A. Shihab, A.-H. Kh. Elttayef, Energy Procedia **157** (2019) 283.
- [49] S. Taha, S. Begum, V.N. Narwade, D. Halge, J.W. Dadge, M.P. Mahabole, R.S. Khairnar, K.A. Bogle, AIP Conf. Proc. **2220** (2020) 20195.
- [50] A. Giampiccolo, D.M. Tobaldi, S.G. Leonardi, B.J. Murdoch, M.P. Seabra, M.P. Ansell, G. Neri, R.J. Ball, Appl. Catal. B Environ. **243** (2019) 183.
- [51] H. Sopha, Y. Norikawa, M. Motola, L. Hromadko, J. Rodriguez-Pereira, J. Cerny, T. Nohira, K. Yasuda, J.M. Macak, Electrochem. Commun. **118** (2020) 106788.
- [52] A.M. Alotaibi, S. Sathasivam, B.A.D. Williamson, A. Kafizas, C. Sotelo-Vazquez, A. Taylor, D.O. Scanlon, I.P. Parkin, Chem. Mater. **30** (2018) 1353.
- [53] A.K. Vishwakarma, L. Yadava, Adv. Sci. Eng. Med. **10** (2018) 723.
- [54] M. Daraee, M. Baniadam, A. Rashidi, M. Maghrebi, Chem. Phys. **511** (2018) 7.
- [55] K.M. Emran, S.M. Ali, H.E. Alanazi, J. Electroanal. Chem. **856** (2020) 113661.
- [56] X. Chang, J. van der Zalm, S.S. Thind, A. Chen, J. Electroanal. Chem. **863** (2020) 114049.
- [57] G.K. Mor, K. Shankar, M. Paulose, O.K. Varghese, C.A. Grimes, Nano Lett. **5** (2005) 191.
- [58] O.K. Varghese, D. Gong, M. Paulose, K.G. Ong, E.C. Dickey, C.A. Grimes, Adv. Mater. **15** (2003) 624.
- [59] P.M. Perillo, D.F. Rodríguez, Chemosensory **4** (2016) 15.
- [60] X. Tian, L. Liu, Y. Li, C. Yang, Z. Zhou, Y. Nie, Y. Wang, Sens. Actuator B Chem. **256** (2018) 135.
- [61] P. Bindra, A. Hazra, Sens. Actuator B Chem. **290** (2019) 684.
- [62] N.D. Chinh, N. Van Toan, V. Van Quang, N. Van Duy, N.D. Hoa, N. Van Hieu, Sens. Actuator B Chem. **201** (2014) 7.
- [63] J.-S. Lee, A. Katoch, J.-H. Kim, S.S. Kim, J. Nanosci. Nanotechnol. **16** (2016) 11580.
- [64] G.-H. Lee, Mater. Res. Innov. **20** (2016) 421.
- [65] S.P. Pishekloo, R.S. Dariani, Appl. Phys. A **122** (2016) 401.
- [66] S.R. Sani, A.M. Ali, R. Jafari, Physica E Low Dimens. Syst. Nanostruct. **43** (2011) 1809.
- [67] K. Huo, X. Zhang, L. Hu, X. Sun, J. Fu, P.K. Chu, Appl. Phys. Lett. **93** (2008) 13105.
- [68] X. Peng, A. Chen, Appl. Phys. A **80** (2005) 473.
- [69] B. Poudel, W.Z. Wang, C. Dames, J.Y. Huang, S. Kunwar, D.Z. Wang, D. Banerjee, G. Chen, Z.F. Ren, Nanotechnology **16** (2005) 1935.
- [70] B. Bhowmik, K. Dutta, N. Banerjee, A. Hazra, P. Bhattacharyya, Nanotechnology **24** (2013) 553.
- [71] M. Epifani, T. Andreu, R. Zamani, J. Arbiol, E. Comini, P. Siciliano, G. Faglia, J.R. Morante, CrystEngComm **14** (2012) 3882.
- [72] J.A. Losilla, C. Ratanatawanate, K.J. Balkus, J. Exp. Nanosci. **9** (2014) 126.
- [73] M.A. Rahman, S. Bazargan, S. Srivastava, X. Wang, M. Abd-Ellah, J.P. Thomas, N.F. Heinig, D. Pradhan, K.T. Leung, Energy Environ. Sci. **8** (2015) 3363.
- [74] A. Nikfarjam, S. Hosseini, N. Salehifar, ACS Appl. Mater. Interfaces **9** (2017) 15662.
- [75] J. Wang, Z. Lin, J. Phys. Chem. C **113** (2009) 4026.
- [76] D. Zhang, Z. Liu, C. Li, T. Tang, X. Liu, S. Han, B. Lei, C. Zhou, Nano Lett. **4** (2004) 1919.
- [77] H.M.M.M. Arachchige, D. Zappa, N. Poli, N. Gunawardhana, N.H. Attanayake, E. Comini, Nanomaterials

- 10** (2020) 935.
- [78] J. Shi, Y. Hara, C. Sun, M.A. Anderson, X. Wang, *Nano Lett.* **11** (2011) 3413.
- [79] H. Wang, Q. Sun, Y. Yao, Y. Li, J. Wang, L. Chen, *Ceram. Int.* **42** (2016) 8565.
- [80] H. Bian, S. Ma, A. Sun, X. Xu, G. Yang, J. Gao, Z. Zhang, H. Zhu, *Superlattices Microstruct.* **81** (2015) 107.
- [81] J.-A. Park, J. Moon, S.-J. Lee, S.H. Kim, T. Zyung, H.Y. Chu, *Thin Solid Films* **518** (2010) 6642.
- [82] S.T. Navale, Z.B. Yang, C. Liu, P.J. Cao, V.B. Patil, N.S. Ramgir, R.S. Mane, F.J. Stadler, *Sens. Actuator B Chem.* **255** (2018) 1701.
- [83] S.G. Pawar, S.L. Patil, M.A. Chougule, B.T. Raut, P.R. Godase, R.N. Mulik, S. Sen, V.B. Patil, *Sens. J.* **11** (2011) 2980.
- [84] B.C. Yadav, S.R. Sabhajeet, R.K. Sonker, *J. Mater. Sci. Res.* **2018** (2018) 114.
- [85] P. Dhivya, A.K. Prasad, M. Sridharan, *Ceram. Int.* **40** (2014) 409.
- [86] M.-H. Seo, M. Yuasa, T. Kida, J.-S. Huh, K. Shimanoe, N. Yamazoe, *Sens. Actuator B Chem.* **137** (2009) 513.
- [87] Z. Zhu, S.-J. Lin, C.-H. Wu, R.-J. Wu, *Sens. Actuator A Phys.* **272** (2018) 288.
- [88] M.-H. Seo, M. Yuasa, T. Kida, J.-S. Huh, K. Shimanoe, N. Yamazoe, *Sens. Actuator B Chem.* **137** (2009) 513.
- [89] O. Alev, E. Şennik, N. Kılınc, Z.Z. Öztürk, *Procedia Eng.* **120** (2015) 1162.
- [90] H. Yang, X.-L. Cheng, X.-F. Zhang, Z. Zheng, X. Tang, Y.-M. Xu, S. Gao, H. Zhao, L.-H. Huo, *Sens. Actuator B Chem.* **205** (2014) 322.
- [91] S. Lin, D. Li, J. Wu, X. Li, S.A. Akbar, *Sens. Actuator B Chem.* **156** (2011) 505.
- [92] P.M. Perillo, D.F. Rodríguez, *Sens. Actuator B Chem.* **171-172** (2012) 639.
- [93] W.-C. Tian, Y.-H. Ho, C.-H. Chen, C.-Y. Kuo, *Sensors* **13** (2013) 865.
- [94] L. Li, Z. Tong, W. Zhi-Jun, L. Shou-Chun, T. Yun-Xia, L. Wei, *Chin. Phys. Lett.* **26** (2009) 90701.
- [95] Y. Luo, C. Zhang, B. Zheng, X. Geng, M. Debliquy, *Int. J. Hydrog. Energy* **42** (2017) 20386.
- [96] F.E. Annanouch, Z. Haddi, M. Ling, F. Di Maggio, S. Vallejos, T. Vilic, Y. Zhu, T. Shujah, P. Umek, C. Bittencourt, C. Blackman, E. Llobet, *ACS Appl. Mater. Interfaces* **8** (2016) 10413.
- [97] X. Yue, S. Jiang, L. Ni, R. Wang, S. Qiu, Z. Zhang, *Chem. Phys. Lett.* **615** (2014) 111.
- [98] B.P. Bastakoti, N.L. Torad, Y. Yamauchi, *ACS Appl. Mater. Interfaces* **6** (2014) 854.
- [99] M.F. Fellah, *Int. J. Hydrog. Energy* **44** (2019) 27010.
- [100] X. Zhang, J. Tie, Q. Chen, P. Xiao, M. Zhou, *IEEE Trans. Dielectr. Electr. Insul.* **22** (2015) 1559.
- [101] X. Xing, N. Chen, Y. Yang, R. Zhao, Z. Wang, Z. Wang, T. Zou, Y. Wang, *Phys. Status Solidi* **215** (2018) 1800100.
- [102] H. Abe, Y. Kimura, T. Ma, D. Tadaki, A. Hirano-Iwata, M. Niwano, *Sens. Actuator B Chem.* **321** (2020) 128525.
- [103] S.S. Rane, S. Arbuj, N. Joshi, R. Ghuge, S.B. Rane, S.W. Gosavi, *Sens. Lett.* **17** (2019) 269.
- [104] D.S. Vlachos, C.A. Papadopoulos, J.N. Avaritsiotis, *Sens. Actuator B Chem.* **44** (1997) 458.
- [105] A. Abbasi, J.J. Sardroodi, *J. Nanostructure Chem.* **7** (2017) 121.
- [106] W. Chomkitichai, N. Tamaekong, C. Liewhiran, A. Wisitsoraat, S. Sriwichai, S. Phanichphant, *Eng. J.* **16** (2012) 135.
- [107] N. Mintcheva, P. Srinivasan, J.B.B. Rayappan, A.A. Kuchmizhak, S. Gurbatov, S.A. Kulinich, *Appl. Surf. Sci.* **507** (2020) 145169.
- [108] Y. Zhang, D. Li, L. Qin, D. Liu, Y. Liu, F. Liu, H. Song, Y. Wang, G. Lu, *Sens. Actuator B Chem.* **255** (2018) 2240.
- [109] J.R. Nataraj, P.Y. Bagali, M. Krishna, M.N. Vijayakumar, *Mater. Today Proc.* **5** (2018) 10670.
- [110] Z. Wang, A.A. Haidry, L. Xie, A. Zavabeti, Z. Li, W. Yin, R.L. Fomekong, B. Saruhan, *Appl. Surf. Sci.* **533** (2020) 147383.
- [111] S. Rahbarpour, S. Sajed, N. Ghodsi, H. Ghafoorifard, *Mater. Res. Express* **6** (2019) 85905.
- [112] E. Şennik, O. Alev, Z.Z. Öztürk, *Sens. Actuator B Chem.* **229** (2016) 692.
- [113] F. Pan, H. Lin, H. Zhai, Z. Miao, Y. Zhang, K. Xu, B. Guan, H. Huang, H. Zhang, *Sens. Actuator B Chem.* **261** (2018) 451.
- [114] D. Zhang, C. Jiang, X. Zhou, *Talanta* **182** (2018) 324.
- [115] R.L. Fomekong, B. Saruhan, *Front. Mater.* **6** (2019) 252.
- [116] M. Kumar, A.K. Gupta, D. Kumar, *Ceram. Int.* **42** (2016) 405.
- [117] A. Monamary, K. Vijayalakshmi, S.D. Jereil, *Physica B Condens. Matter* **553** (2019) 182.
- [118] L. Xie, Z. Li, L. Sun, B. Dong, Q. Fatima, Z. Wang, Z. Yao, A.A. Haidry, *Front. Mater.* **6** (2019) 96.
- [119] B.C. Sertel, H.I. Efkere, S. Ozcelik, *IEEE Sens. J.* **20** (2020) 13436.
- [120] D. Mardare, N. Cornei, C. Mita, D. Florea, A. Stancu, V. Tiron, A. Manole, C. Adomnitei, *Ceram. Int.* **42** (2016) 7353.
- [121] D. Mardare, C. Adomnitei, D. Florea, D. Luca, A. Yildiz, *Physica B Condens. Matter* **524** (2017) 17.
- [122] X. Tong, W. Shen, X. Zhang, J.-P. Corriou, H. Xi, J. Alloys Compd. **832** (2020) 155015.
- [123] J. Wu, D. Zhang, Y. Cao, *Colloid Interface Sci.* **529** (2018) 556.
- [124] R.L. Fomekong, K. Kelm, B. Saruhan, *Sensors* **20** (2020) 5992.
- [125] K. Vijayalakshmi, A. Monamary, *J. Mater. Sci. Mater. Electron.* **27** (2016) 140.
- [126] V. Galstyan, E. Comini, C. Baratto, A. Ponzoni, M. Ferroni, N. Poli, E. Bontempi, M. Brisotto, G. Faglia, G. Sberveglieri, *Sens. Actuator B Chem.* **209** (2015) 1091.
- [127] V. Galstyan, A. Ponzoni, I. Kholmanov, M.M. Natile, E. Comini, G. Sberveglieri, *Sens. Actuator B Chem.* **303** (2020) 127217.
- [128] Z. Li, Z. Yao, A.A. Haidry, T. Plecenik, B. Grancic, T. Roch, M. Gregor, A. Plecenik, *J. Alloys Compd.* **806** (2019)

1052.

- [129] A. Abbasi, J.J. Sardroodi, *Comput. Theor. Chem.* **1095** (2016) 15.
- [130] W. Pan, Y. Zhang, D. Zhang, *Appl. Surf. Sci.* **527** (2020) 146781.
- [131] D. Zhang, X. Zong, Z. Wu, Y. Zhang, *Sens. Actuator B Chem.* **266** (2018) 52.
- [132] S.B. Eadi, S. Kim, S.W. Jeong, H.W. Jeon, *Adv. Mater. Sci. Eng.* **2017** (2017) 2191659.
- [133] Z. Li, A.A. Haidry, T. Wang, Z.J. Yao, *Appl. Phys. Lett.* **111** (2017) 32104.
- [134] Y. Bao, P. Wei, X. Xia, Z. Huang, K. Homewood, Y. Gao, *Sens. Actuator B Chem.* **301** (2019) 127143.
- [135] Y. Gönüllü, A.A. Haidry, B. Saruhan, *Sens. Actuator B Chem.* **217** (2015) 78.
- [136] L. Zhu, D. Zhang, Y. Wang, C. Feng, J. Zhou, C. Liu, S. Ruan, *RSC Adv.* **5** (2015) 28105.
- [137] M. Saberi, A.L.I.A. Ashkarran, *Surf. Rev. Lett.* **24** (2017) 1850024.
- [138] L. Wang, X. Xing, N. Chen, R. Zhao, Z. Wang, T. Zou, W. Zhezhe, Y. Wang, *J. Nanostructures* **10** (2020) 148.
- [139] S.R. Sabhajeet, R.K. Sonker, B.C. Yadav, *Adv. Sci. Eng. Med.* **10** (2018) 736.
- [140] D.N. Suryawanshi, I.G. Pathan, A.R. Bari, L.A. Patil, *J. Eng. Sci.* **11** (2020) 1242.
- [141] M.A. Kaiyum, N. Ahmed, A. Alam, M.S. Rahman, *Res. Square* (2020) 1.
- [142] Z.P. Tshabalala, K. Shingange, F.R. Cummings, O.M. Ntwaeaborwa, G.H. Mhlongo, D.E. Motaung, *J. Colloid Interface Sci.* **504** (2017) 371.
- [143] Y. Zhang, Q. Yang, X. Yang, Y. Deng, *Microporous Mesoporous Mater.* **270** (2018) 75.

(Rec. 02/01/2021, Rev. 24/02/2021, Ac. 01/03/2021)

